

## POLARIMETRY MICROLENSING OF CLOSE-IN PLANETARY SYSTEMS

SEDIGHE SAJADIAN<sup>1</sup>, MARKUS HUNDERTMARK<sup>2,3</sup>

*Draft version June 28, 2021*

### Abstract

A close-in giant planetary (CGP) system has a net polarization signal whose value varies depending on the orbital phase of the planet. This polarization signal is either caused by the stellar occultation or by reflected starlight from the surface of the orbiting planet. When the CGP system is located in the Galactic bulge, its polarization signal becomes too weak to be measured directly. One method for detecting and characterizing these weak polarization signatures due to distant CGP systems is gravitational microlensing. In this work, we focus on potential polarimetric observations of highly-magnified microlensing events of CGP systems. When the lens is passing directly in front of the source star with its planetary companion, the polarimetric signature caused by the transiting planet is magnified. As a result some distinct features in the polarimetry and light curves are produced. In the same way microlensing amplifies the reflection-induced polarization signal. While the planet-induced perturbations are magnified, whenever these polarimetric or photometric deviations vanish for a moment the corresponding magnification factor or the polarization component(s) is equal to the related one due to the planet itself. Finding these exact times in the planet-induced perturbations helps us to characterize the planet. In order to evaluate the observability of such systems through polarimetric or photometric observations of high-magnification microlensing events, we simulate these events by considering confirmed CGP systems as their source stars and conclude that the efficiency for detecting the planet-induced signal with the state-of-the-art polarimetric instrument (FORS2/VLT) is less than 0.1%. Consequently, these planet-induced polarimetry perturbations can likely be detected under favorable conditions by high-resolution and short-cadence polarimeters of the next generation.

*Keywords:* Gravitational lensing; micro; techniques: polarimetric, planetary systems.

### 1. INTRODUCTION

The scattering of photons in stellar atmospheres creates linearly polarized light. Due to the circular symmetry of the surface of stars, the net polarization signal is zero (Chandrasekhar 1960; Sobolev 1975). In various types of stars, different physical scattering mechanisms can produce a non-vanishing local polarization signal (see e.g. Ingrosso et al. 2012). In the hot early-type stars, for instance, Thompson scattering in their atmospheres generates polarized light (Chandrasekhar 1960). For late-type main-sequence stars, the polarization is caused by both Rayleigh scattering on neutral hydrogens and to a lesser degree by Thompson scattering by free electrons (Fluri & Stenflo 1999; Stenflo 2005). In cool giant stars, Rayleigh scattering on atomic and molecular species or on dust grains generates the polarization.

During a microlensing event, the circular symmetry of images breaks causing a time-dependent net polarization signal for the source star (Schneider & Wagoner 1987; Simmons et al. 1995a,b; Bogdanov et al. 1996). The exact value of this polarization depends on the minimum distance between lens and source center with respect to the source radius in addition to the source type. It reaches its maximum value when  $u \approx 0.96\rho_*$  in microlensing events caused by single microlenses, where  $u$

is the projected lens-source distance normalized to the Einstein radius and  $\rho_*$  is the source radius projected on the lens plane and normalized to the Einstein radius. The Einstein radius is the radius of the ring of images when the lens, source and observer are completely aligned. For early-type source stars this maximal contribution is 0.6 – 0.7% which is measurable with state-of-the-art polarimeters, such as the FOcal Reducer and low dispersion Spectrograph (FORS2) polarimeter at Very Large Telescope (VLT) telescope.

Measuring the polarization signal during microlensing events helps to constrain the finite source size, the Einstein radius and the limb-darkening parameters of the source star surface (Yoshida 2006; Agol 1996; Schneider & Wagoner 1987). Moreover, lensing can magnify the intrinsic polarization of source stars and make them detectable through polarimetric microlensing. Different kinds of anomalies on the surface or in the atmosphere of a source star can lead to a net polarization. Magnetic fields those are distributed over the surface of a source star can cause polarization through two channels of the Zeeman effect and breaking the circular symmetry of the source surface brightness due to their temperature contrasts. Photometric observations are more efficient in detecting stellar spots than polarimetric observations, but by using polarimetric observations we can estimate the magnetic field of source star spots (Sajadian 2015). Circumstellar hot disks around the microlensed stars located at the Galactic bulge lead to net polarization signals for their host stars due to their projected elliptical shapes. Indeed, these distant disks are unresolvable from their host stars. Polarimetric mi-

s.sajadian@cc.iut.ac.ir

<sup>1</sup> Department of Physics, Isfahan University of Technology, Isfahan 84156-83111, Iran

<sup>2</sup> Astronomisches Rechen-Institut, Zentrum für Astronomie der Universität Heidelberg (ZAH), 69120 Heidelberg, Germany

<sup>3</sup> Niels Bohr Institute & Centre for Star and Planet Formation, University of Copenhagen Øster Voldgade 5,1350-Copenhagen,Denmark

cro lensing observations of these systems can offer a lower limit to the disk inner radius (Sajadian & Rahvar 2015). In addition, rapid stellar rotation makes (i) stars oblate which breaks the spherical symmetry of the source and (ii) the gravity-darkening effect which breaks the respective circular symmetry of the stellar surface brightness. Hence, stellar rotation can also lead to a net polarization depending on the inclination angle of its rotational axis as well as its angular speed. The corresponding stellar ellipticity causes some time shifts in the peak positions of the polarimetry and light curves of high-magnification microlensing events. Measuring these shifts can only viably achieved by using polarimetric microlensing (Sajadian 2016).

A distant CGP system has also a net polarization signal which varies with time while the planet is orbiting its host star. This polarization signal can be caused by (i) the reflection of the stellar light from the planet surface (e.g. Seager et al. 2000), (ii) the stellar occultation by the transiting planet (e.g. Carciofi & Magalhães 2005) or (iii) the planet occultation by the source edges while the planet is occulted by its host star. The polarization signal due to the reflection is maximal when the phase angle is about 90 degree, where the phase angle is measured between the source and Earth as seen from the planet center and the occultation polarization is maximal when the planet is crossing the source edges. As a side-remark, the polarization caused by the occultation of the planet by the star is maximal in the infrared bands and its duration is too short. Generally, the total polarization signal due to a distant CGP system is too low to be directly measured. Again, microlensing can magnify all these effects of close-in giant planets orbiting source stars beyond the detection limit.

The detectability of such CGP systems in microlensing events through pure photometric observations were studied in great details. For instance, Graff & Gaudi (2000) proposed detecting Jupiter-size planets around the source stars during caustic-crossing microlensing events. This aspect was further addressed by Sajadian & Rahvar (2010) who studied the efficiency of detecting such systems as a function of wavelength. Microlensing light curves of transiting planets orbiting source stars were studied by Rybicki & Wyrzykowski (2014) and they have concluded that the probability for detecting a transiting planet in a given microlensing event is of the order of  $2 \times 10^{-6}$ . We propose *polarimetric observations* as a new channel for detecting and even characterizing such systems in the Galactic bulge through high-magnification or caustic-crossing microlensing events. The outline of this paper is as follows: in the next section, we first outline our framework for describing a planetary orbit and its projection on the sky for applying the lensing formalism. Then, we explain how to calculate the net polarization signal of a CGP system. In section (3), we study the polarimetric microlensing signatures of these systems. Finally, we discuss on probability of detecting CGP systems through photometric or polarimetric observations of high-magnification caustic-crossing microlensing events in section (5).

## 2. POLARIZATION SIGNAL OF A DISTANT CGP SYSTEM

In this section, we outline the formalism for calculating the polarization signal of a CGP system. First, we in-

roduce the relevant parameters and coordinate systems to establish a planetary orbit. Then, we assess different contributions to the net polarization signal of a CGP system.

### 2.1. Kepler parameters for a planetary orbit

The Kepler problem of a planetary system whose components interact through their gravitational force is converted to motion of an object with the reduced mass  $\mu = M_\star M_p / (M_\star + M_p)$  around their center of mass over an ellipse, where  $M_p$  and  $M_\star$  are the masses of the planet and its parent star respectively. The radial distance of the reduced mass relative to the center of mass is given by (e.g. Landau & Lifshitz 1969, Smart 1980):

$$r(\xi) = a(1 - e \cos \xi), \quad (1)$$

where  $a$  is the semi-major axis and  $e$  is the orbital eccentricity.  $\xi$  is called the true anomaly and its dependence on time is given by the Kepler equation:

$$\xi - e \sin \xi = \omega(t - t_p) = \phi, \quad (2)$$

where  $\omega = 2\pi/T$  is the orbital angular velocity,  $T = 2\pi\sqrt{a^3/G(M_\star + M_p)}$  is the orbital period and given by the Kepler's third law and  $t_p$  is the time of the perihelion passage. The Kepler equation can be numerically solved by using a series expansion of the Bessel functions (Watson 1966; Nucita et al. 2014):

$$\xi = \phi + \sum_{n=1}^{+\infty} \frac{2}{n} J_n(ne) \sin(n\phi), \quad (3)$$

where  $J_n(ne)$  is the Bessel function of the order  $n$ . The radial motion of the planet around its host star is given by  $r_p = r(\xi)\mu/M_p$ .

We define a Cartesian coordinate system  $(x_p, y_p, z_p)$  with the origin at the center of the source star. Its  $y_p$  and  $z_p$ -axes coincide with the orbital plane and point towards the semi-major and minor axes respectively. The  $x_p$ -axis is orthogonal to this plane, so that all basis vectors form a right-handed system. In this coordinate system, the components of the position of the planet center at each time is given by (e.g. Dominik 1998):

$$\begin{aligned} y_{c,p} &= \frac{\mu}{M_p} a (\cos \xi - e), \\ z_{c,p} &= \frac{\mu}{M_p} a \sqrt{1 - e^2} \sin \xi, \\ x_{c,p} &= 0. \end{aligned} \quad (4)$$

We also consider an observer coordinate system describing the sky plane  $(x_o, y_o, z_o)$  with the origin at the center of the source star. In this coordinate system, the  $y_o$  and  $z_o$ -axes are on the sky plane and its  $x_o$ -axis points towards the observer. In order to convert the first coordinate system to the second one, we first need to rotate the planetary orbital plane around the  $x_p$ -axis by the angle  $\beta$  which is the angle between the semi-major axis of the planetary orbit with respect to the intersection line of the sky plane and the orbital plane. Then, we project the planetary orbit on the sky plane by rotating it around the semi-major axis of the planetary orbit by the inclination angle  $i$  which is the angle between its semi-minor axis and sky plane.

Based on these coordinate systems, the phase angle i.e. the angle between the source star and the observer as seen from the planet center, is given by:  $\cos \alpha = -x_{c,o} / \sqrt{x_{c,o}^2 + y_{c,o}^2 + z_{c,o}^2}$ , where  $(x_{c,o}, y_{c,o}, z_{c,o})$  describes the position of the planet center at each time in the observer coordinate system:

$$\begin{aligned} y_{c,o} &= \cos \beta y_{c,p} + \sin \beta z_{c,p}, \\ z_{c,o} &= -\cos i \sin \beta y_{c,p} + \cos i \cos \beta z_{c,p}, \\ x_{c,o} &= \sin i \sin \beta y_{c,p} - \sin i \cos \beta z_{c,p}. \end{aligned} \quad (5)$$

In order to describe each point on the planet surface, we require a third coordinate system  $(x', y', z')$  with the origin at the planetary center. The  $x'$ -axis is pointing towards the host star, the  $y'$ -axis is contained in the plane  $x_o - x'$  and its  $z'$ -axis is normal to the plane  $x' - y'$ , so that one gets a right-handed system. Each point on the planet surface in this system is given by:

$$\begin{aligned} x' &= R_p \sin \theta \cos \phi, \\ y' &= R_p \sin \theta \sin \phi, \\ z' &= R_p \cos \theta, \end{aligned} \quad (6)$$

where  $R_p$  is the planet radius,  $\theta$  and  $\phi$  are the polar and azimuthal angles on the planetary surface. In order to convert this coordinate system to the observer's system, we first rotate the coordinate system around the  $z'$ -axis by the phase angle  $\alpha$ . Then, we rotate the resulting system around its  $x'$ -axis by  $-\gamma$ , where  $\gamma = \cos^{-1}(y_{c,o} / \sqrt{x_{c,o}^2 + y_{c,o}^2 + z_{c,o}^2})$  is the angle between the line pointing towards the center of the planet and the  $y_o$ -axis as seen from the host star.

Light coming from a CGP system located in the Galactic bulge is linearly polarized which is due to (i) the reflection of the host star light in the planetary atmosphere, (ii) the stellar occultation by the transiting planet or (iii) the planetary occultation by the source star. The latter is negligible given the faintness of the planet itself. We will expand on the two relevant components of the polarization in the following.

## 2.2. Polarization due to reflection

The polarization caused by reflected starlight in a CGP system is a well-studied phenomenon. Chandrasekhar (1950,1960) and Horak & Chandrasekhar (1961) have analytically solved the radiative transfer equations to calculate the intensity and the state of polarization of the light reflected by a semi-infinite homogeneous plane-parallel atmosphere in the context of conservative and non-conservative Rayleigh scattering. Subsequently, many researchers have applied Chandrasekhar's approaches to the polarimetry of exo-planets (e.g. Natraj et al. 2009, Kane & Gelino 2010).

Under the assumption of radiative equilibrium, for a given chemistry and sources of absorption and scattering, Seager et al. (2000) have presented light and polarimetry curves of a CGP system. Moreover, many numerical models have been developed to calculate the polarization and intensity of light reflected by planets (see e.g. Sengupta & Maiti 2006, Stam 2008, Buenzli & Schmid 2009, Cahoy et al. 2011, Kostogryz et al. 2011, Whitney 2013). Indeed, the reflected

light by a planet is significantly polarized, whereas the direct light from the host star is generally unpolarized due to the symmetry of the stellar surface brightness. Accordingly, polarimetry was recommended as a method for detecting and characterizing Jupiter-like planets (Hough & Lucas 2003; Stam et al. 2004).

In this work, we use the analytical framework developed by Madhusudhan & Burrows (2012) to calculate the Stokes parameters (Stokes 1852; Tinbergen 1996), which was based on the Chandrasekhar (1950,1960)'s approach assuming a cloud-free homogeneous (in the scattering albedo) and semi-infinite atmosphere.

The left panel of Figure (1) shows the time-dependent polarization signal due to the reflected light from the planet surface. This figure is similar to the bottom panel of Figure (4) of Madhusudhan & Burrows (2012). However, the scales are different because we normalize the polarized flux to the total flux due to the planet and its host star, whereas in the mentioned reference the polarized flux is normalized to the flux of the planet itself. According to this figure, the polarization curve due to the reflection has two peaks when  $\alpha \sim 90^\circ$ . The polarization curves are plotted for three different values of the planet semi-major axis  $a = 0.008$  A.U. (red solid),  $a = 0.01$  A.U. (green dashed) and  $a = 0.02$  A.U. (red dotted) and three different inclination angles  $i = 80, 40, 10$  degree from thickest lines to thinnest lines respectively. The vertical black dashed lines show the source radius. Consequently, the polarization signal is detectable while the planet is out of the source surface and it does not transit its host star, except for the small inclination angles. Closer planets lead to higher reflection polarizations. The small black features in this figure represent the polarization signal due to the planet occultation by its host star for  $a = 0.008$  A.U. and  $i = 80^\circ$ . This polarization occurs whenever the planet is behind its host star surface and in that case the contribution is small.

## 2.3. Polarization due to the stellar occultation by planet

The occultation of the source surface by its planet breaks the circular symmetry of the stellar surface brightness and produces a linear polarization signal. The value of this polarization is maximal when the planet is crossing the edge of the source (Carciofi & Magalhães 2005; Wiktorowicz & Laughlin 2014; Kostogryz et al. 2015). However, the occultation happens for phase angles greater than  $90^\circ$  (i.e. when the planet is passing in front of the source star) as well as when  $R_{c,o} < R_\star + R_p$ , where  $R_\star$  is the source radius and  $R_{c,o} = \sqrt{z_{c,o}^2 + y_{c,o}^2}$  is the projected radial distance of the planet center with respect the source center. The stellar occultation only happens when the inclination angle is greater than:  $i \geq \cos^{-1}(R_s + R_p)/b_p$ , where  $b_p$  is the semi-minor axis of the planetary orbit after rotating the orbital plane by  $\beta$ . Our formalism for calculation of the occultation polarization is similar to the one introduced by Carciofi & Magalhães (2005). The only difference is that we consider a non-circular planetary orbit and as a result we need two rotation angles to project the planetary orbit onto the sky plane. Whereas in the aforementioned reference only circular planetary orbits were considered which need just a single projection angle.

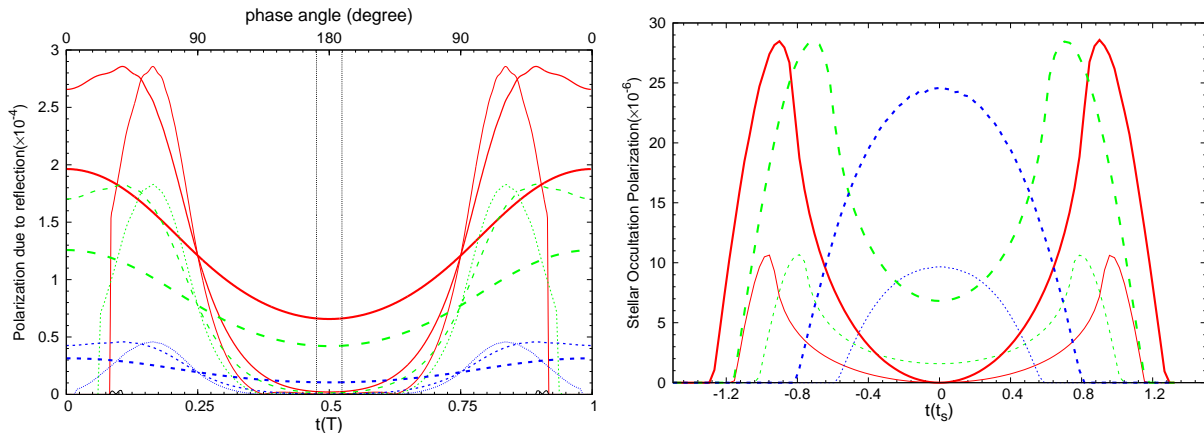


**Figure 1.** The polarization signal of a CGP system is shown. Left panel: the time-dependent polarization signal due to the reflected light from the planet (normalized to the planetary orbital period  $T$ ). The polarizations are plotted for three different values of the planet semi-major axis  $a = 0.008$  A.U. (red solid),  $a = 0.01$  A.U. (green dashed) and  $a = 0.02$  A.U. (blue dotted) and three different inclination angles  $i = 80, 40, 10$  degree from thickest lines to thinnest lines respectively. Right panel: the polarization signal due to the occultation of the source surface by the planet versus time (normalized to source crossing time by planet  $t_s$ ). The polarimetry curves are plotted for two values of the planet radius  $R_p = R_J$  (thin curves) and  $R_p = 2R_J$  (thick curves) and three different inclination angles  $i = 90$  degree (red solid),  $75^\circ$  (green dashed) and  $63^\circ$  (blue dotted).

A stellar occultation inevitably leads to a linear polarization. The right panel of Figure (1) represents the time-dependent polarization signal due to the occultation of the source surface by the planet expressed in the unit of the source star crossing time (i.e.  $t_s = T R_*/(2\pi a)$ ). The polarimetry curves are plotted for two values of the planet radius  $R_p = R_J$  (thin curves) and  $R_p = 2R_J$  (thick curves) and three different inclination angles  $i = 90$  degree (red solid),  $75^\circ$  (green dashed) and  $63^\circ$  (blue dotted). According to this figure, the polarimetry curve due to the occultation has one or two peaks, which all happen when the planet is crossing the source edge. The time interval between these peaks depends on the inclination angle. This figure is similar to the figure (4) of Carciofi & Magalhães (2005). However, the semi-major axis of the planet orbit in our calculation is 0.25 times smaller. In addition, we have considered different wavelengths.

### 3. HIGH-MAGNIFICATION MICROLENSING OF A CGP SYSTEM

In this section, we study polarimetric microlensing events of the CGP system that was discussed in the previous section. In these kind of events we encounter two time-dependent properties: (i) the lens distance from the planetary system and (ii) the position of the planet with respect to its host star. We focus on close-in planetary systems, because for these systems the effect of the reflected light from the planet surface is considerably higher and the probability that the planet transiting the source star is high. These CGP systems have time-dependent intrinsic polarization signals which are likely not detectable when these systems are located in the Galactic bulge. Lensing can magnify these low polarization signals if (i) the angular separation between lens and CGP system is very small (i.e. fractions of a mas) or (ii) if this system passes the caustic of a multiple-lens system. In the following subsections, we analyze how lensing changes the occultation and reflection polarizations respectively and focus on the first scenario.

#### 3.1. Lensing of the occultation polarization

In a high-magnification microlensing event of a CGP system in which the lens passes the source surface, the

occultation signature is most likely magnified and causes some photometry and polarimetry deviations in the related curves.

In order to formulate the polarization signal, we use the Stokes parameters  $S_I$ ,  $S_Q$ ,  $S_U$  and  $S_V$  which describe the total intensity, two components of linear polarized intensities and the circular polarized intensity over the source surface respectively (Tinbergen 1996). The scattering process produces linear polarizations on the source surface, so we set  $S_V = 0$ . The other Stokes parameters are calculated by integrating of the total and polarized flux over the source surface and by considering the magnification factor for each element of the source surface:

$$S_{I,*} = \int_0^1 \rho d\rho \int_{-\pi}^{\pi} d\phi F^*(\mu) A(u), \quad (7)$$

$$\begin{pmatrix} S_{Q,*} \\ S_{U,*} \end{pmatrix} = \int_0^1 \rho d\rho \int_{-\pi}^{\pi} d\phi F_p^*(\mu) A(u) \begin{pmatrix} -\cos 2\phi \\ \sin 2\phi \end{pmatrix},$$

where  $\rho$  is the distance from the center to each projected element over the source surface normalized to the source radius,  $\mu = \sqrt{1 - \rho^2}$ ,  $\phi$  is the azimuthal angle between the lens-source connection line and the line from the center to each element over the source surface,  $u$  is the distance of each projected element over the source surface with respect to the lens position and  $A(u)$  is the magnification factor. Noting that the Stokes parameters are normalized to  $R_*^2$ . The total and polarized fluxes ( $F^*$ ,  $F_p^*$ ) depend on the type of the source star and its temperature (see e.g. Ingrassio et al. 2012,2015).

Let us assume the source star is a transiting CGP system. In that case the total stokes parameters are divided into two parts, the first part ( $S_{I,*}, S_{Q,*}, S_{U,*}$ ) is the total Stokes parameters contribution due to the source star itself and the second part ( $S_{I,p}, S_{Q,p}, S_{U,p}$ ) is the contribution by the planet which is evaluated by integrating over the planet surface considering the total and polarized fluxes of its host star at the planet location. Consequently, the total Stokes parameters ( $S'_I, S'_Q, S'_U$ ) are given by:

$$S'_i = R_*^2 S_{i,*} - R_p^2 S_{i,p}, \quad (8)$$

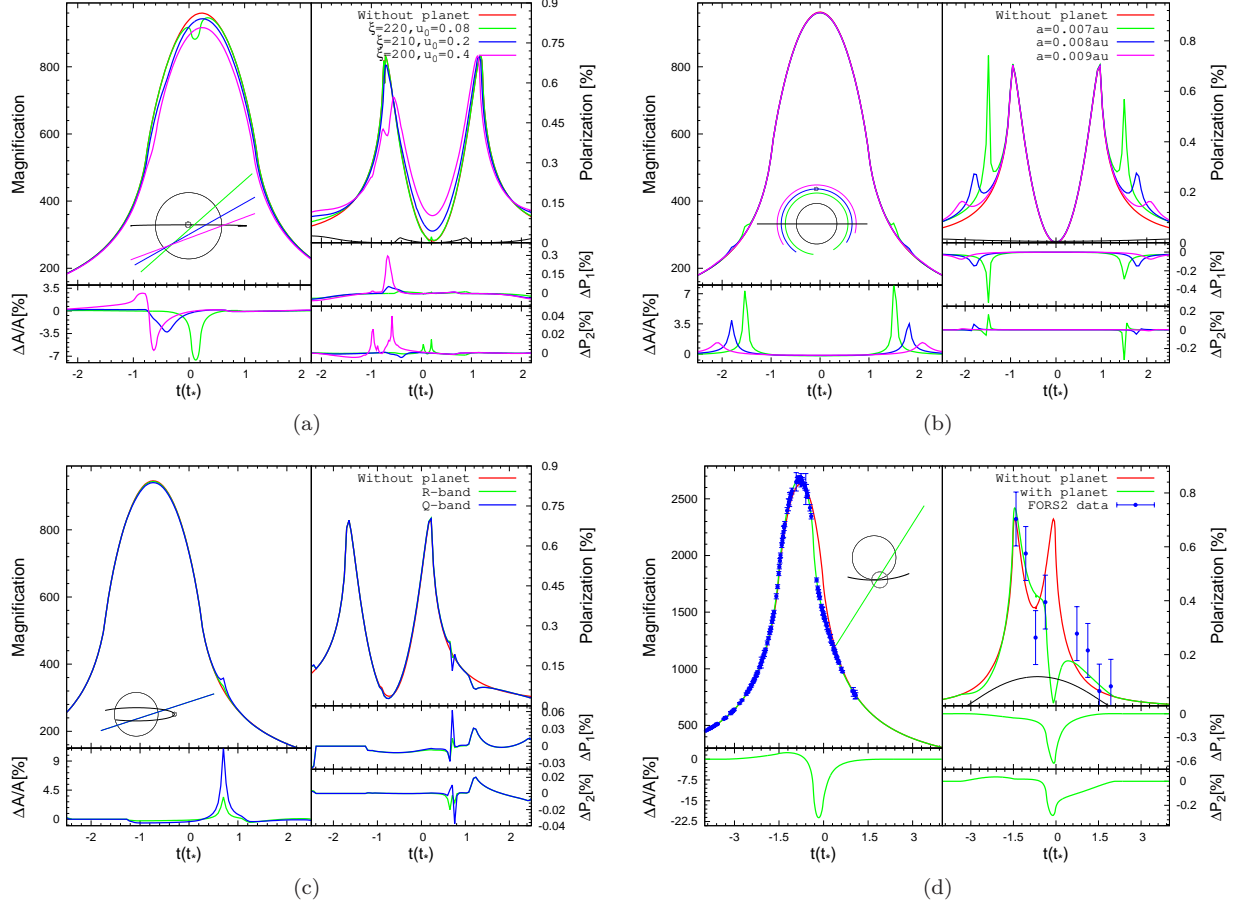


**Figure 2.** Typical high-magnification microlensing events of CGP systems. In each subfigure, light and polarimetric curves are shown in the left and right panels respectively. The source and its planet (black and gray circles), the projected path of the planet around its host star (solid gray lines) and the lens trajectories (color lines) are shown in the inset in the left-hand panels. Simple models without a planetary perturbation are plotted with red solid lines. The black thinner curves in the right panels represent the intrinsic polarization signals of the CGP systems varying with time. The photometric and polarimetric residuals with respect to the simple models are shown in the lower panels. The parameters used to make these figures are reported in Table (1).

where  $i \in (I, Q, U)$ . The planet Stokes parameters ( $S_{I,p}, S_{Q,p}, S_{U,p}$ ) depend on the location of the planet on the source surface with respect to the lens position and the planet size. We assume that the observation is carried out in the optical band, so that the thermal radiation of the planet is negligible.

The magnification factor of such a CGP system is given by:

$$A' = \frac{S_{I,*} - \delta S_{I,p}}{S_{I,*0} - \delta S_{I,p,0}} = A \frac{1 - \delta S_{I,p}/S_{I,*}}{1 - \delta S_{I,p,0}/S_{I,*0}}, \quad (9)$$

where the index 0 of the Stokes parameters refers to the contribution without lensing effect and  $\delta = R_p^2/R_*^2$  represents the ratio of the planet area to its host star area. The parameters with denoted with a prime contain the polarimetric signal caused by the transiting planet. As expected, the relative size of the planet to the source star is an important factor in the magnitude of the perturbation due to a transiting planet.

When the lens is approaching the source star surface and resides far from the transiting planet, the planet-induced deviation in the photometry curve is positive, because the term  $S_{I,*}$  is magnified significantly. The second term  $S_{I,p}$  will be magnified whenever the

lens approaches the planet position or is crossing the planet surface resulting a negative deviation in the light curve. Whenever the total deviation vanishes, i.e.  $S_{I,p}/S_{I,*} = S_{I,p,0}/S_{I,*0}$ , the magnification factor is equal to the magnification factor of the source star without the planet and also equals to the magnification of the planet itself  $A' = A = A_p = S_{I,p}/S_{I,p,0}$ .  $A_p$  depends on the location of the planet with respect to the source center and its size. Let us assume the lens position can be deduced from photometric measurements. The magnification factor in this case gives us some information on the planet characteristics. Generally, depending on the lens and planet trajectories over the source surface the planet-induced deviations can have different shapes. For instance, they could be always negative (or always positive).

We can write the polarization vector as  $P' = (S'_Q/S'_I, S'_U/S'_I)$  whose components are given by:

$$\begin{aligned} P'_1 &= P_1 \frac{1 - \delta S_{Q,p}/S_{Q,*}}{1 - \delta S_{I,p}/S_{I,*}}, \\ P'_2 &= P_2 \frac{1 - \delta S_{U,p}/S_{U,*}}{1 - \delta S_{I,p}/S_{I,*}}. \end{aligned} \quad (10)$$

The planet-induced polarimetric perturbations can also be in the form of positive and negative deviations. Similarly, whenever these deviations in each polarization component vanishes while the lens is magnifying the transiting planet effect, we will have  $P'_1 = P_1 = P_{1,p} = S_{Q,p}/S_{I,p}$  or  $P'_2 = P_2 = P_{2,p} = S_{U,p}/S_{I,p}$ . The value of that polarization component at that time gives us one constraint on the properties of the planet.

Figure 2(a) shows a high-magnification microlensing of a CGP system, while the lens is passing the source surface. The photometric and polarimetric curves are plotted in the left and right panels. The simple models without any planet around the source star are shown with a red solid line, the photometric residual  $\Delta A = (A' - A)/A$  and the polarimetric residuals in the polarization components  $\Delta P_{1,2} = P'_{1,2} - P_{1,2}$  (in %) are plotted in the lower panels. The thin curve in the right-handed plot shows the intrinsic polarization signal due to the CGP system which varies with the time. According to this figure, the maximum photometric deviation due to the stellar occultation is achieved when the lens approaches the planet while it is crossing the source center. The maximum polarimetric deviation occurs if the lens approaches the planet which is passing the edge of the source. Because the peak of the total stellar flux, considering limb-darkening, comes from the center of the source, the stellar polarized flux maximizes at the source edges. The polarimetric perturbations due to a transiting planet are located over (or between) the polarimetric maxima. Here, the inclination angle of the planetary orbit is about  $90^\circ$ , so that the reflection and occultation polarizations are separated in time, and thus just the occultation polarization is magnified. However, when the inclination angle is lower the reflection and occultation polarizations can coincide.

### 3.2. Lensing of the reflection polarization

When the lens is passing very close to the source star it may pass close to the planet and results the reflection polarization signal to be magnified. In that case, the total Stokes parameters are given by:

$$S'_i = R_\star^2 S_{i,\star} + R_p^2 S_{i,r}, \quad (11)$$

where  $i \in (I, Q, U)$ ,  $S_{i,r}$  is the total Stokes parameter due to the reflected light by the planet and is obtained by integrating over the illuminated part of the planet surface which is a function of the phase angle. Accordingly, the magnification factor in a high-magnification microlensing event of a CGP system, while the lens is magnifying the reflected light by the planet atmosphere will be:

$$A' = A \frac{1 + \delta S_{I,r}/S_{I,\star}}{1 + \delta S_{I,r,0}/S_{I,\star,0}}. \quad (12)$$

The factors  $S_{I,r}/S_{I,\star}$  and  $S_{I,r,0}/S_{I,\star,0}$  are proportional to the ratio of the source flux reflected by the planet atmosphere to the total source flux, i.e.

$$F^r/F^\star = A_g \left(\frac{R_p}{a}\right)^2 \Phi(\alpha),$$

where  $A_g$  is the geometrical albedo which is the fraction of the incident reflected light from the planet surface at

the phase angle equal to zero.  $\Phi(\alpha)$  is the phase function and indicates the fraction of the planet surface that is illuminated by the source star and can be detected by the observer. In these cases, some positive or negative deviations can appear in an unperturbed light curve. Whenever the planet-induced deviation vanishes for a moment (i.e.  $S_{I,r}/S_{I,\star} = S_{I,r,0}/S_{I,\star,0}$ ) we have  $A' = A = A_r$ , where  $A_r = S_{I,r}/S_{I,r,0}$  is the magnification factor of the planet itself by considering its reflected radiation. Also, the polarization components are given by:

$$\begin{aligned} P'_1 &= P_1 \frac{1 + \delta S_{Q,r}/S_{Q,\star}}{1 + \delta S_{I,r}/S_{I,\star}}, \\ P'_2 &= P_2 \frac{1 + \delta S_{U,r}/S_{U,\star}}{1 + \delta S_{I,r}/S_{I,\star}}. \end{aligned} \quad (13)$$

It is clear that the planet-induced deviations in the polarization components can also be in the form of positive or negative deviations with respect to the unperturbed polarization components of the source star. If at some time between these deviations in each polarization component the perturbation effect vanishes, then  $P'_1 = P_1 = P_{1,p} = S_{Q,r}/S_{I,r}$  or  $P'_2 = P_2 = P_{2,p} = S_{U,r}/S_{I,r}$ . Consequently, when the lens is passing close to the planet, its reflected light will be magnified. In the resulting photometric or polarimetric deviations, the times when these deviations vanish give us some information about the planet characteristics.

Figure 2(b) represents a polarimetric microlensing event of a CGP system for three different values of the planet semi-major axis. In these events the reflected light by the planet is passing close to the lens. Here the positive-negative transitions happen in the second component of the stellar polarization. By increasing the planet distance from its host star the contribution of the reflected light significantly decreases.

There is another polarization signal in a micro-lensed CGP system which is due to being magnified the thermal radiation from the planet itself. This component is considerably stronger in infrared bands and depends on the planet's temperature which is given by:

$$T_p = T_\star (R_\star/a)^{1/2} (f(1 - A_b))^{1/4},$$

where  $f$  is the redistribution factor which describes the fraction of re-radiating energy which is absorbed by the planet and  $A_b$  is the bond albedo (or spherical albedo) which is the total fraction of incident light reflected by a sphere at all angles. We indicate the geometrical and bond albedos according to the amount of the scattering albedo  $A_s$  (Madhusudhan & Burrows 2012). In Figure 2(c) we show a high-magnification microlensing event of a CGP system in two different pass bands. In this event, we align the lens trajectory so that it reaches to the planet when the phase angle  $\sim 120^\circ$ , i.e. the contributions of the occultation and reflection polarizations is negligible. According to this figure the planet-induced perturbation due to the thermal radiation of the planet increases with increasing the wavelength.

There is a twofold degeneracy in these kinds of events. If  $u_0 \rightarrow -u_0$  and  $i \rightarrow -i$ , the photometric and polarimetric curves do not change, but the polarimetric angle  $\theta'_p = 1/2 \tan^{-1}(S'_U/S'_Q)$  converts to  $180 - \theta'_p$ . Hence, in

**Table 1**

The parameters of microlensing events shown in Figures 2(a), 2(b), 2(c) and 2(d).

	$M_p(M_J)$	$R_p(R_J)$	$a(\text{A.U.})$	$i^\circ$	$u_0(\rho_*)$	$\xi^\circ$	$t_0(t_*)$	$t_p(T)$
2(a)	0.4	0.9	0.008	89	--	--	0.23	-0.25
2(b)	0.4	0.9	--	10	0.009	180	0	-0.25
2(c)	0.5	1.0	0.008	80	-0.2	18	-0.73	0
2(d)	0.68	1.2	0.05	41	0.6	296	-0.46	-0.24

**Note.** — The columns contains (i) the figure, (ii) the planet mass  $M_p(M_J)$ , (iii) the planet radius  $R_p(R_J)$ , (iv) the semi-major axis  $a(\text{A.U.})$ , (v) the inclination angle of the planetary orbital plane with respect to the sky  $i^\circ$ , (vi) the impact parameter of the lens trajectory with respect to the source center normalized to  $\rho_*$   $u_0(\rho_*)$ , (vii) the angle of the lens trajectory with respect to the semi-major axis of the planetary orbit  $\xi^\circ$ , (viii) the time of the closest approach of the lens trajectory with respect to the source center in the unit of the crossing time of the source surface  $t_0(t_*)$  and (ix) the time of the perihelion passage in the planetary orbit in the unit of the orbital period  $t_{0,p}(T)$  respectively. The other parameters are fixed: the mass of the source star  $M_* = M_\odot$ , the radius of the source star  $R_* = R_\odot$ , the lens mass  $M_l = 0.3 M_\odot$ , the lens and source distances from the observer  $D_l = 6.5$  kpc,  $D_s = 8.0$  kpc, the limb-darkening coefficients  $c_1 = 0.64$ ,  $c_2 = 0.032$ , the redistribution factor  $f = 2/3$ , the eccentricity of the planetary orbit  $e = 0$ , the projection angle of the planetary semi-major axis with respect to the sky plane  $\beta = 0^\circ$  and the scattering albedo in the planet atmosphere  $A_s = 0.9$ .

these microlensing events polarimetric observations resolve the twofold degeneracy which is not doable relying on photometric observations alone. This is one of the major advantages of polarimetric observation of high-magnification or caustic-crossing microlensing events.

Let us assume the lens is a binary system also and the source star is also a CGP system. In these events, while the source star is passing the caustic its planet can cross the caustic lines several times and as a result some periodic perturbations will appear in the related curves. The orbital period of the CGP system can be measured through an accurate timing analysis of the residuals. This method was proposed for measuring the orbital period in the close binary microlensing events by Nucita et al. (2014). The important issue in this regard is that the time scale of these planet-induced perturbations is too short and is of the order of  $t_p = t_E \rho_p$ , where  $\rho_p$  is the projected planet radius on the lens plane and normalized to the Einstein radius. This issue decreases the probability of measuring these period perturbations. However, this polarimetry time scale will be considerable in long-duration microlensing events only. Also, in binary microlensing events of CGP systems, we can obtain some information about the planet from the times when the planet-induced perturbations vanishes for a moments in the polarimetry or light curves, same as single-lens microlensing events.

#### 4. OBSERVABILITY OF CGP SYSTEMS IN HIGH-MAGNIFICATION MICROLENSING EVENTS

In this section, we investigate the polarimetric and photometric efficiencies for detecting the CGP system signatures in high-magnification microlensing events. We first study the statistical contribution of the intrinsic polarization signals due to observed CGP systems which have been mostly found by the transit method and are available online on the NASA's exoplanet archive<sup>4</sup>. Based on our selection of CGPs, we simulate high-magnification microlensing events with source star CGPs and provide detection probabilities for the photometric and polarimetric signature.

<sup>4</sup> <http://exoplanetarchive.ipac.caltech.edu/>

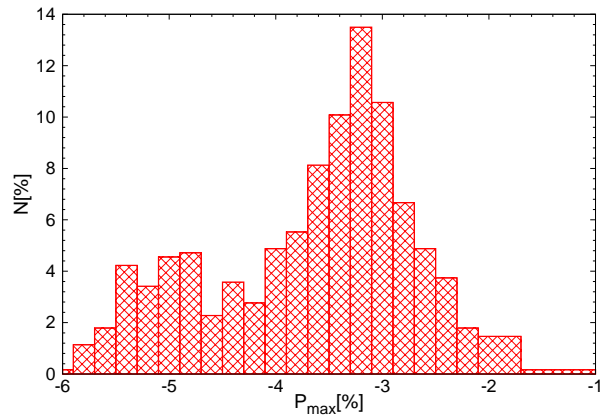


**Figure 3.** The distribution of the maximum polarization signals (in %) due to the confirmed CGP systems with semi-major axes with less than 0.07 A.U..

There are about 615 confirmed close-in giant planets with measured semi major-axes  $< 0.07$  A.U. which have been detected with various methods. We choose these transiting CGP systems for simulating source stars and randomly pick the inclination angles ( $\beta, i$ ) and calculate their maximum polarization signals. Figure (3) shows the distribution of the maximal detectable polarization signature caused by these CGP systems. We find that the net polarization cause by these systems is very low and mostly less than  $10^{-3}\%$ . The reflection polarization signals due to CGP systems can reach  $10^{-3}\%$  and correspond to the second peak in the Figure (3). The occultation polarizations are even weaker and of the order of  $10^{-5}\%$  which correspond to the first deviating peak. About 2% of CGP systems have a maximum polarization signal greater than 0.01%.

Then, we simulate high-magnification microlensing events of these CGP systems to assess the polarimetry and photometry efficiencies for detecting planet-induced signatures in these events. We envisage polarimetric observations of these high-magnification microlensing events are carried out using the FORS2 instrument at the VLT and according to the observational strategy of this instrument simulate the observational data points.

Further details on simulating polarimetric microlensing observations with FORS2 can be found in the work by Sajadian (2016). One example of such a simulated polarimetric microlensing event of a CGP system is shown in Figure 2(d). In this event, the planet-induced polarimetric perturbation exceeds the polarimetric accuracy of FORS2 i.e. 0.1%. The cadence of FORS2 observations is about 20 min and thus exceeds the time-scale of the polarimetric perturbation, so that the polarimetric data points can not cover the second polarimetric peak and resolve the planet-induced perturbation. The photometric signature of the planet is very small, but high spatial resolution of the photometric observations and the short cadence leave the planet-induced perturbation detectable.

In about 10% of the simulated events, the lens distance from the planet decreases to less than  $\sim 4\rho_p$ . For 3% of our simulated events the photometric signatures of the close-in planet around the source star are detectable with  $\Delta\chi^2 > 50$ , where  $\Delta\chi^2 = \chi_p^2 - \chi_s^2$  is the change in  $\chi^2$  for a fitted microlensing light curve with and without CGP system orbiting the source. The polarimetric perturbations were not detectable in any simulated event for that criterion. It means that the polarimetric efficiency for detecting CGP systems in high-magnification microlensing events is less than 0.1% for one state-of-the-art instrument with a corresponding polarimetric accuracy of 0.1% and an observational cadence about 20 min. Consequently, as expected the photometry observations are more efficient for detecting CGP systems around the source stars than the polarimetry observations.

The small polarimetry efficiency for detecting CGP systems orbiting the source stars is not only owing to the low polarimetry precision of FORS2 but also more due to the long necessary observational time for taking one polarimetry data point by FORS2. Regarding the second issue, the FORS2 cadence (about 20 min) is of the order of the time scale of the planet-induced polarimetry perturbations (i.e.  $t_p = \rho_p t_E$ ) which causes a lack of enough number of the polarimetry data points to cover these perturbations, as shown in Figure 2(d). It means that if several high resolution polarimeters observe high-magnification microlensing events synchronously, the polarimetry efficiency for detecting this kind of perturbations significantly increases.

However, the advantages of potential high-resolution and short-cadence polarimetry observations in near future from high-magnification microlensing events of CGP systems will be (i) resolving the twofold degeneracy which is not resolvable by doing photometry observations alone and (ii) obtaining some extra information about the planet through the times in which the planet-induced perturbations vanishes for an instance, as explained in the previous section.

## 5. CONCLUSIONS

More than 600 close-in giant planetary (CGP) systems with semi-major axes less than 0.07 A.U. have been confirmed up to now. Most of the detected systems are closer than 1 kpc from us and were often detected by the transit method. CGP systems located in the Galactic bulge distance can be detected only through gravitational microlensing. Finding such systems in the Galactic bulge would help us to study the distribution of such systems

in different environments and understand the environmental effect on the formation of these systems.

One method for detecting CGP systems through gravitational microlensing is polarimetry observations. In that case, planetary signatures can be magnified beyond a common detection threshold if (i) a high-magnification microlensing event occurs or (ii) if the system crosses a caustic line. Unmagnified CGP systems will also lead to a net polarization signal, albeit too small to be measured directly. During a high-magnification or caustic-crossing microlensing event, the undetectable polarization signal can be magnified which causes deviations in their polarimetric curves and was discussed in this work. The polarization signal itself is caused by the stellar occultation by the planet or by the reflection of the host star's light from the planet surface and strongly depends on the orbital radius, the density and surface area of the planet and the chemical components in the planetary atmosphere. Polarization by reflection exceeds the signal caused by the primary transit by about two orders of magnitude.

While the lens is crossing the source star surface, the occultation polarization is likely to be magnified and when the lens is sufficiently close to the source star and out of its surface, the reflection polarization can be magnified, too. The resulting perturbations do not have commonly identifiable shapes, because lens and planet trajectories can come in a variety of configurations. But in all cases of these photometric or polarimetric perturbations, finding the times when the polarimetric or photometric perturbation vanishes gives some information about the planet.

We have also investigated the observability of detecting photometric and polarimetric deviations in the related curves of high-magnification microlensing events of a sample of confirmed CGP systems in NASA's exoplanet database. We conclude that the photometric efficiency for detecting these signatures is about 3%, whereas the polarimetric efficiency is less than 0.1% which is comparable to state-of-the-art instruments with a polarimetric accuracy 0.1%. The small polarimetry efficiency for detecting CGP systems orbiting the source stars is owing to the low polarimetry precision of FORS2 and rather due to the long necessary observational time for taking one polarimetry data point by FORS2. If several high resolution polarimeters observe high-magnification microlensing events synchronously, the polarimetry efficiency for detecting this kind of perturbations significantly increases. However, the advantages of high-resolution and short-cadence polarimetry observations in near future from high-magnification microlensing events of CGP systems will be (i) resolving the twofold degeneracy which is not resolvable by doing photometry observations alone and (ii) getting some extra information about the planet through the times in which the planet-induced perturbations vanishes for an instance.

We are thankful from N. Kostogryz for providing her results of simulating the center-to-limb polarization profile in continuum spectra of low-mass stars. We would like to thank the anonymous referee for his/her helpful



comments and suggestions.

## REFERENCES

- Agol, E. 1996, *MNRAS*, 279, 571
- Bogdanov, M. B., Cherepashchuk, A. M. & Sazhin, M. V. 1996, *Ap&SS*, 235, 219
- Buenzli, E., & Schmid, H. M. 2009, *A&A*, 504, 259
- Cahoy, K. L., Marley M. S., Fortney J. J. 2011, *ApJ*, 724, 189
- Carciofi, A. C. & Magalhães, A. M. 2005, *ApJ*, 635, 570
- Chandrasekhar, S. 1950, *Radiative Transfer* (Oxford, Clarendon Press)
- Chandrasekhar, S. 1960, *Radiative Transfer* (New York, Dover Publications)
- Dominik, M. 1998, *A&A*, 329, 361
- Fluri, D. M., Stenflo, J. O. 1999, *A&A*, 341, 902
- Graff, D. S., & Gaudi, B. S. 2000, *ApJ*, 538, 133
- Hough, J. H. & Lucas, P. W. 2003, in *Proc. Conf. Towards Other Earths*(ESA SP-539), ed. M. Fridlund, & T. Henning (Noordwijk: ESA), 11
- Horak, H. G., & Chandrasekhar, S. 1961, *ApJ*, 134, 45
- Ingrosso, G., Calchi Novati, S., De Paolis, F., et al. 2012, *MNRAS*, 426, 1496
- Ingrosso G., Calchi Novati S., De Paolis, F., et al. 2015, *MNRAS*, 446, 1090
- Kane, S. R., & Gelino, D. M. 2010, *ApJ*, 724, 818
- Kostogryz, N. M., Yakobchuk, T. M., Morozhenko, O. V., & Vid'machenko, A. O. 2011, *MNRAS*, 415, 695
- Kostogryz, N. M., Yakobchuk, T. M., & Berdyugina, S. V. 2015, *ApJ*, 806, 97
- Landau, L. D., Lifshitz, E. M. 1969, *Mechanics*, 2nd Edition (Oxford, Pergamon Press)
- Madhusuhan, N. & Burrows, A. 2012, *ApJ*, 747, 25
- Natraj, V., Li K-F., Yung, Y. L. 2009, *ApJ*, 691, 1909
- Nucita, A. A., Giordano, M., De Paolis, F., Ingrosso, G. 2014, *ApJ*, 438, 2466
- Rybicki, K. & Wyrzykowski, L. 2014, *A&A*, 64, 65
- Sajadian, S., & Rahvar, S. 2010, *MNRAS*, 407, 373
- Sajadian, S. 2015, *MNRAS*, 452, 2587
- Sajadian, S. & Rahvar, S. 2015, *MNRAS*, 454, 4429
- Sajadian, S. 2016, *ApJ*, 826, 152
- Schneider, P., Wagoner, R. V. 1987, *ApJ*, 314, 154
- Seager, S., Whitney, B. A. & Sasselov, D. D. 2000, *ApJ*, 540, 504
- Sengupta, S., & Maiti, M. 2006, *ApJ*, 639, 1147
- Simmons, J. F. L., Newsam, A. M. & Willis, J. P. 1995a, *MNRAS*, 276, 182
- Simmons, J. F. L., Willis, J. P., Newsam, A. M. 1995b, *A&A*, 293, 46
- Smart, W. M. 1980, *Textbook on Spherical Astronomy* (Cambridge, Cambridge University Press)
- Sobolev, V. V. 1975, *Light Scattering in Planetary Atmospheres* (Pergamon Press, Oxford)
- Stam, D. M., Hovenier, J. W. & Waters B. F. M. 2004, *A&A*, 428, 663
- Stam, D. M. 2008, *A&A*, 482, 989
- Stenflo, J. O. 2005, *A&A*, 429, 713
- Stokes, G. G. 1852, *TCaPS*, 9, 399
- Tinbergen, J. 1996, *Astronomical Polarimetry* (New York, Cambridge University Press)
- Watson, G. N. 1966, *A Treatise on the Theory of Bessel Functions*, (Cambridge, Cambridge University Press)
- Whitney, B. A., et al. 2013, *ApJS*, 207, 30
- Wiktorowicz, S. J., & Laughlin, G. P. 2014, *ApJ*, 795, 12
- Yoshida, H. 2006, *MNRAS*, 369, 997